True-time-delay modules based on a single tunable laser in conjunction with a waveguide hologram for phased array antenna application

Zhong Shi
Lanlan Gu, MEMBER SPIE
Brie Howley, MEMBER SPIE
Yongqiang Jiang, MEMBER SPIE
QingJun Zhou
Ray Chen, FELLOW SPIE
The University of Texas at Austin
Department of Electrical and Computer Engineering
Microelectronics Research Center
Austin, Texas 78758
E-mail: raychen@uts.cc.utexas.edu

Yihong Chen
Xiaodong Wang
Omega Optics, Inc.

H. R. Fetterman
University of California
Los Angeles

George Brost
Air Force Research Lab

Abstract. A wavelength-controlled continuous beam-steering four-element X-band (8- to 12-GHz) phased array antenna system is presented. The system is based on the continuously tunable optical true-time-delay technique. Dispersion-enhanced waveguide holograms were proposed and used to fabricate the optical true-time-delay devices. The devices are characterized both theoretically and experimentally. The wavelength of a laser was tuned within the system to get continuously tunable true time delay. The time delay was measured for a wavelength tuning range from 1537 to 1547 nm in 10-nm steps. The far-field radiation patterns of the antenna system were measured at 9 and 10.3 GHz, and they showed no beam squint. The true-time-delay formation idea presented here is suitable for not only X-band, but also for higher microwave frequencies, such as K-band. [DOI: 10.1117/1.2009766]

Subject terms: antenna systems; waveguides; true-time-delay modules.

Paper 040141 received Mar. 15, 2004; revised manuscript received Nov. 24, 2004; accepted for publication Feb. 16, 2005; published online Aug. 10, 2005.

1 Introduction

Phased array antennas consist of a large number of discrete radiating elements that radiate individually and coherently. The far-field radiation pattern of such antennas is determined by the amplitude and phase of the excitation sources on each radiating element and the geometric spacing of the elements. The phased array antenna is one of the key technologies in modern surveillance radars and communication systems. It offers advantages such as quick, accurate beam steering without physical movement. The conformal-mounting structure of the radiating elements is another advantage of the phased array antenna. Real applications of large phase-shifter arrays have not been successful, due to the difficulties in integrating thousands of phase shifters into a system in view of weight, cost, and flexibility issues. Another problem in phase-shifter-based phased array antennas is the so-called beam squint effect: The beam pointing direction is different for different microwave carrier frequencies. This effect should be eliminated in wideband antenna systems. Optical true-time-delay techniques have the potential to eliminate the beam squint effect, because the beam-steering direction of the phased array antennas is determined only by the time delay between the different optical elements. With optical techniques, optical carrier frequencies are modulated by the microwave signals and then transmitted or distributed to the receiver ends, which convert the optical signals back to microwave electrical signals. The converted microwave electrical signals are amplified by electrical amplifiers and then fed to the radiation antenna elements. The microwave signals are radiated coherently to the outside at the final stage of the phased array antenna system. Phased array antennas based on optical true time delay are essentially wideband-based systems. So the optical true-time-delay techniques are desirable for applications in modern wideband phased-array antennas. Because the optical carriers modulated by the microwave signals are transmitted via fibers, the noise from the external electromagnetic interference and internal electromagnetic coupling can be greatly reduced. Some optical true-time-delay schemes have been proposed and demonstrated.[1–3] However, most of them are based on discrete true time delay, and continuously tunable optical true-time-delay techniques have rarely been reported so far. Previously we reported an optical continuous true-time-delay formation scheme by tuning different wavelengths within the different true-time-delay modules.[4] However, the proposed structure requires an array of lasers with discrete wavelengths having sufficient temporal synchronization. It may be difficult to

0091-3286/2005/$22.00 © 2005 SPIE

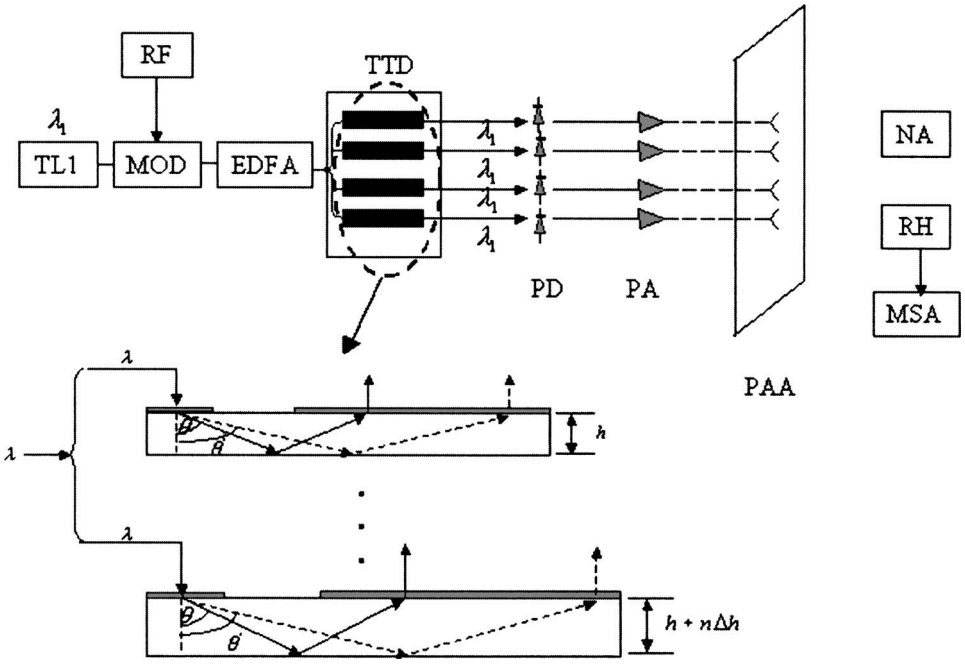

Fig. 1 Schematic of the system experimental setup. Inset is the true-time-delay formation structure. TL: tunable laser; MOD: modulator; EDFA: erbium-doped fiber amplifier; TTD: true-time delay modules; PD: photodetector; PA: postamplifier; PAA: phased array antenna head; NA: network analyzer; RH: receiving horn antenna; MSA: microwave spectrum analyzer.

implement in real application, for each module will need a separate laser. In this paper, we report a single-laser-based structure to continuously form the true time delay for beam steering in a phased array antenna system. The complexity and the cost of the whole system are greatly reduced. The presented true-time-delay technique is based on a dispersion-enhanced waveguide-hologram technique. The true-time-delay formation scheme and the characteristics of the hologram-waveguide-based true-time-delay devices are explained in detail. A four-element phased array antenna system was developed for the microwave X band (8 to 12.5 GHz). We provide experimental results on the wavelength-controlled true time delay and the far-field radiation patterns of the system.

2 True-Time-Delay Module

The true-time-delay formation scheme is shown in the inset of Fig. 1, in which waveguide-hologram strips have thicknesses $h, h+\Delta h, \ldots, h+n\,\Delta h$. A holographic grating is fabricated on top of each strip, and the grating structure of the each strip is exactly the same. For vertically incident

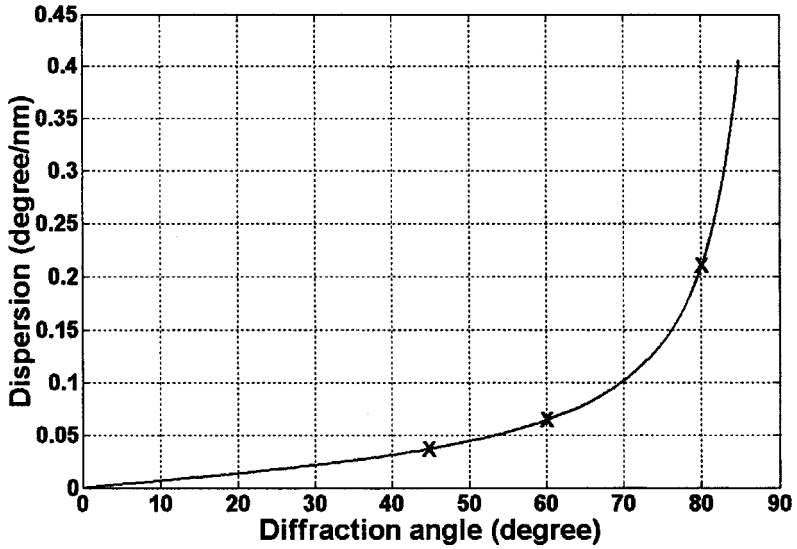

Fig. 2 Calculated dispersion capability at different diffraction angles.

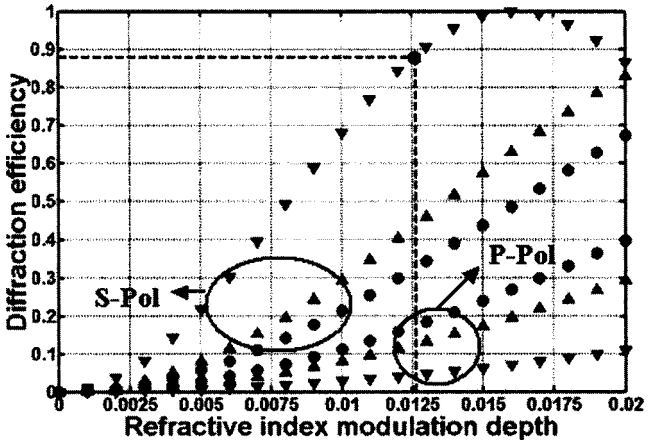

Fig. 3 Calculated diffraction efficiency for S and P polarization at the diffraction angles of 45, 60, and 80 deg.

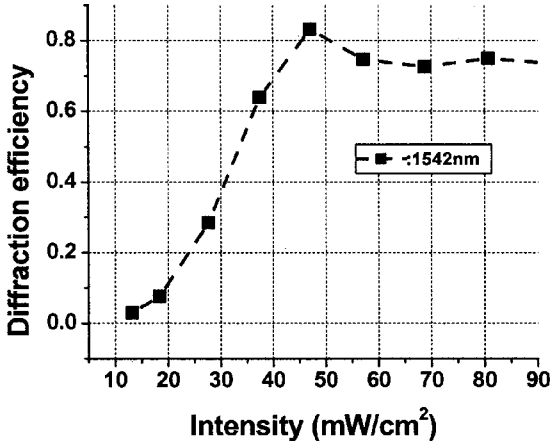

Fig. 5 Measured diffraction efficiency for different recording intensities.

beams, they have the same diffraction angles within the strips. There is a time delay ΔT between the adjacent outputs when the beams are coupled out from the hologram waveguides. For outputs having only one bounce within the glass strips, ΔT is determined to be

$$\Delta T = \frac{2n\,\Delta h}{c\cos\theta}, \tag{1}$$

where n is the refractive index of the glass, Δh is the thickness difference between the adjacent strips, c is the speed of light, and θ is the diffraction angle of the incident beam of wavelength λ within the glass strips. The overall time delay is determined by these parameters. The diffraction angle θ is a function of the incident wavelength λ. A dispersion equation can be derived as follows[5]:

$$\frac{\Delta\theta}{\Delta\lambda} = \frac{\tan\theta}{\lambda}. \tag{2}$$

By tuning the incident wavelength λ, the diffraction angle θ can be changed continuously, thereby making the true time delay continuously tunable. So the dispersion capability of

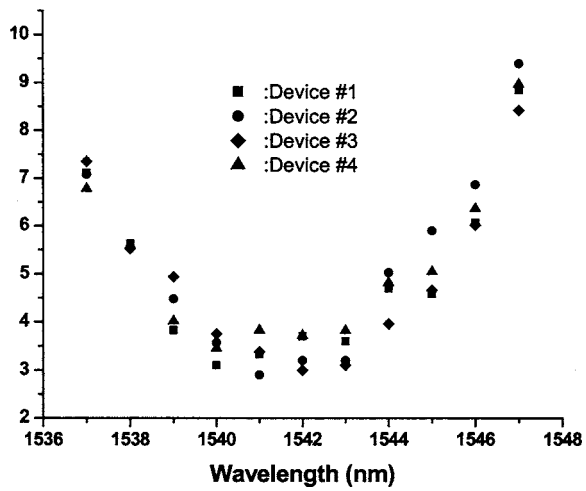

Fig. 6 Measured insertion loss of the devices.

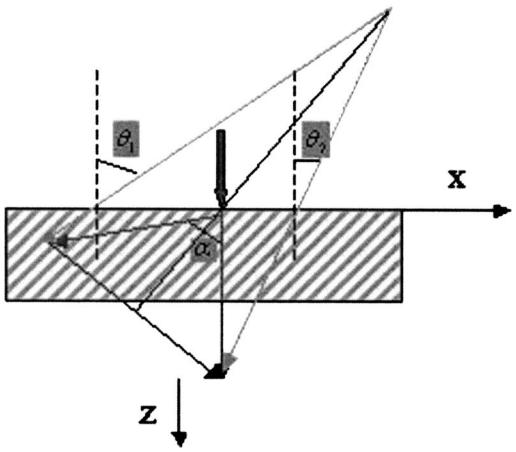

Fig. 4 Diagram for phase-matched condition.

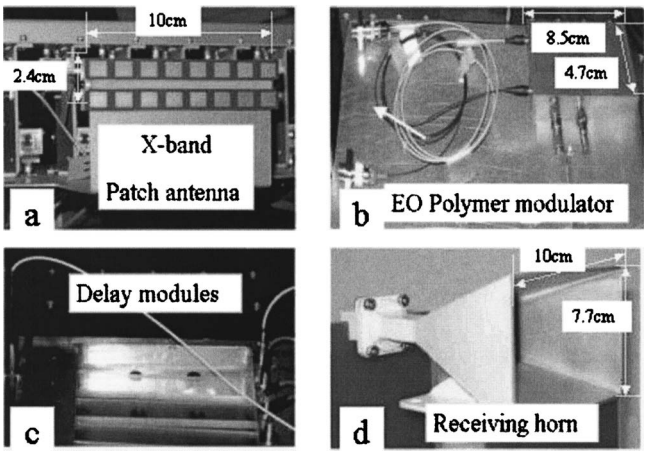

Fig. 7 (a) Patched antenna. (b) Intensity modulator. (c) True-time-delay modules. (d) Receiving horn.

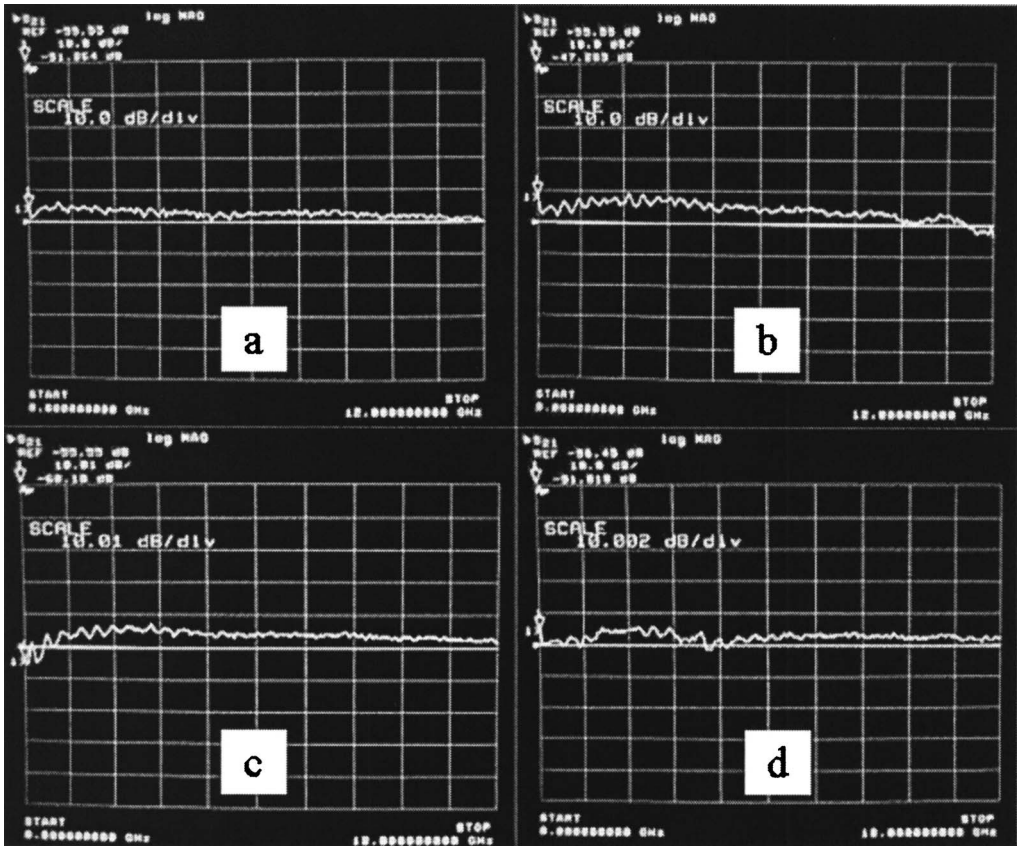

Fig. 8 Measured transmission performance of the four different devices (a, b, c, d) after photodetectors.

the holographic grating is critical to form the time delay in the proposed scheme.

The dispersion equation shows explicitly that the dispersion capability of the holographic grating is directly proportional to the diffraction angle θ for a particular wavelength λ. Thus increasing the diffraction angle will help to increase the dispersion of the grating. On the other hand, the sizes of the devices will be increased when the dispersion capability is increased. Considering the trade-off between the dispersion capability and the sizes of the devices, a diffraction angle of 80 deg at 1542 nm was chosen. Figure 2 shows the dispersion (degrees per nanometer) versus the wavelength shift at different diffraction angles. Three angles are marked in the curve: 45, 60, and 80 deg. Waveguide holograms with diffraction angles of 45 and 60 deg were previously fabricated in our lab for other applications. It can be seen that the dispersion capability at the diffraction angle of 80 deg can be increased by 3.27 times over that at 60 deg and by 5.67 times over that at 45 deg. In the calculation, the wavelength is shifted in steps of 10 nm from 1537 to 1547 nm, and 1537 nm is chosen as reference zero point.

Beside the enhanced dispersion capability, another advantage of the diffraction angle of 80 deg is that the S-polarization components of the incident beams have much higher peak diffraction efficiencies in the 1550-nm region than for diffraction angles from 45 to 60 deg. The theoretical analysis of the diffraction efficiency is based on the coupled-wave theory.[5] The following equations are used to calculate the diffraction efficiency of volume holographic grating.

$$\eta_s = \frac{[\sin(\nu^2 + \xi^2)^{1/2}]^2}{1 + (\xi^2/\nu^2)}, \tag{3}$$

$$\nu = \frac{\kappa_s d}{(C_R C_S)^{1/2}}, \tag{4}$$

$$\xi = -\frac{\Delta\lambda\, k^2 d}{8\pi n C_S} = \frac{\Delta\theta\, kd \sin(\varphi - \theta)}{2C_S}, \tag{5}$$

$$C_R = \cos\,\theta, \quad C_S = \cos\,\theta - \frac{K\cos\,\varphi}{k}, \tag{6}$$

$$\kappa_s = \pi\Delta n/\lambda, \tag{7}$$

where Δn is the amplitude of the refractive index modulation, θ is the incident Bragg angle measured in the hologram medium, which is zero for our design, $\Delta\theta$ is the deviation of the incident angle from the Bragg angle, which is also zero for our design, d is the thickness of the holographic grating layer, λ is the free-space wavelength of the incident light, n is the average refractive index of the grat-

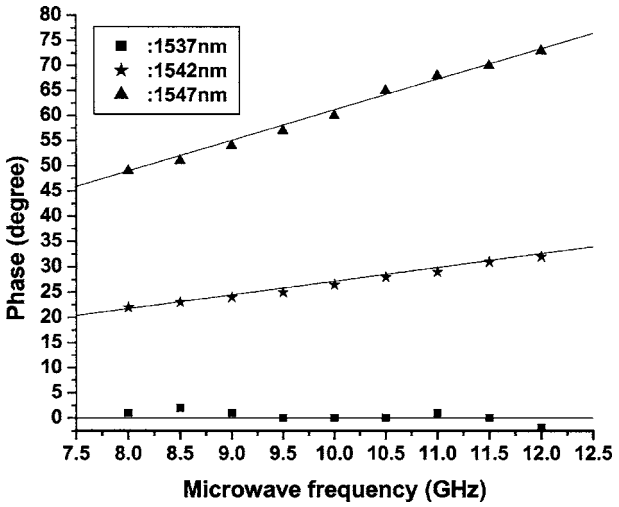

Fig. 9 Measured phase versus frequency curves across X band.

ing medium, φ is the slant angle of the grating with respect to the medium boundaries, K is the magnitude of the grating vector and is equal to $2\pi/\Lambda, \Lambda$ is the grating period, and k_s is the propagation constant of the light inside the medium.

Figure 3 shows the calculated diffraction efficiency at the three diffraction angles 45, 60, and 80 deg. Both S and P polarization components are calculated for each diffraction angle. The horizontal axis is the modulation depth of the refractive index of the photopolymer material. For the material used in the experiment, the refractive index has a maximal modulation depth of about 0.012. It is easy to see that the diffraction efficiency for the S polarization component of the incident beam increases dramatically from ≈35% to ≈87% with the diffraction angle increased from 45 to 80 deg, while the diffraction efficiency of the P polarization component has a relatively flat diffraction efficiency. An intuitive explanation of the increased polarization dependence of the device with increasing diffraction angle is that the incident angle relative to the orientation of grating fringes is made closer and closer to the Brewster angle when the diffraction angle is increased from 45 to 80 deg. Generally speaking, the fibers used within the phased array antenna system are not very long (tens of meters). The polarization-maintaining scheme should have acceptable cost in practice.

The holographic gratings were formed on top of the glass waveguides with a standard two-beam interference setup using Dupont photopolymer with a film thickness of 20 μm. The presence of air ($n=1$) on top of the photopolymer ($n=1.5$) limits the maximum available diffraction angle (≈60 deg) of the recorded grating when the photopolymer is directly exposed to the recording beams,[6] as is illustrated in Fig. 4. In Fig. 4, the maximum achievable θ_1 is about 41 deg if the recording beams shine directly on the photopolymer film. Considering this θ_1 value, the known wave vectors for the recording beam and the playback beam, and some algebraic relationships, it is easy to find that maximum achievable diffraction angle is about 60 deg when the recording beam shines directly on the photopolymer film. So a right-angle prism was placed on top of the photopolymer to increase the maximum achievable θ_1 to record at 80-deg diffraction angle. A Verdi laser with a wavelength of 532 nm is used for recording. The recording process was optimized at different exposure intensities to get the maximal diffraction efficiency.

The optimization result is shown in Fig. 5. The horizontal axis is the intensity of the recording beam, and the vertical axis is the diffraction efficiency achieved. A maximum peak diffraction efficiency of about 83% was achieved at

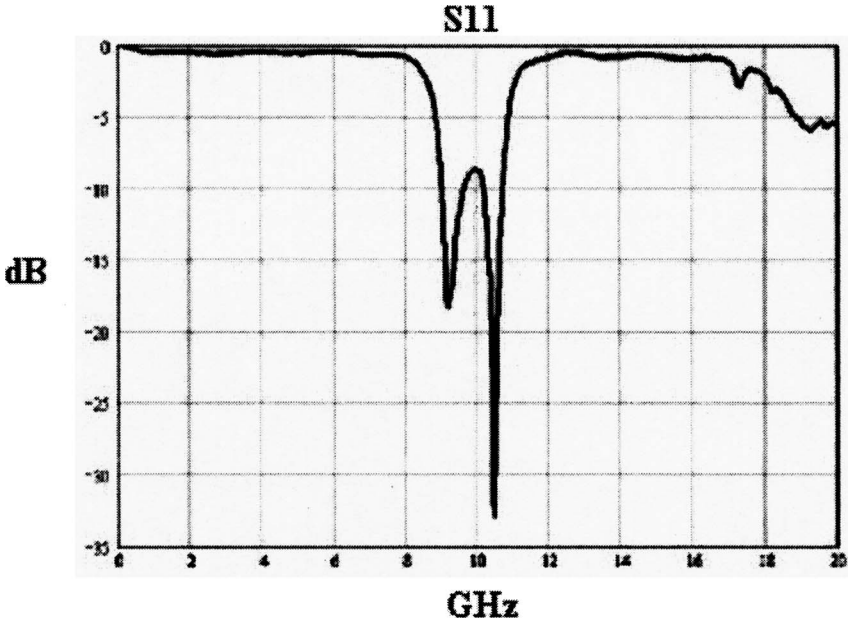

Fig. 10 Measured reflection performance S_{11} of the antenna element.

1542 nm. The recording intensity is 47 mW/cm^2, and the exposure time is 20 s at the optimized diffraction efficiency point.

The measured total insertion loss for the four devices across a 10-nm tuning range is shown in Fig. 6. The rolloff of the curves is due to the limited bandwidth of the holographic grating with a diffraction angle of 80 deg. The loss at 1547 nm is higher than expected, which is due to the noise from scattering beams during the recording process, reducing the diffraction efficiency. The nonuniformity of the four curves and the small ripple of each curve are partly caused by the photopolymer material itself. As the amplitude of the devices will affect the radiation patterns, we are still working on optimization of the amplitude uniformity.

3 System Experiment

The schematic of the experimental setup is shown in Fig. 1. A tunable laser was intensity-modulated by an external intensity modulator, into which the X-band microwave signal was injected from a HP network analyzer (8510C). An erbium-doped fiber amplifier was used after the modulator to compensate the loss in the modulator. The amplified optical signal passed through a 1×4 optical power splitter. After the splitter, the optical signals were injected into the four true-time-delay modules, respectively. The thinnest device has a thickness of 1.2 mm, and the thickness difference is 1.5 mm. After appropriate time delay, the four optical signals were converted to the corresponding electrical signals by four photodetectors. Four electrical amplifiers were used to amplify the electrical signals after the photodetectors. The four amplified electrical signals were delivered to four X-band phased array patched antenna elements. The radiation signal was received by a horn antenna, and the power of the received signal was measured by a microwave spectrum analyzer. The true-time-delay information was analyzed by measuring the relative phase difference between adjacent electrical signals using the network analyzer. Figure 7(a)–7(d) show the antenna head, intensity modulator, true-time-delay modules, and receiving horn used in the experiment, respectively.

The amplitude and the phase of each delay branch affect the radiation pattern of the whole system. The power after the photodetectors was adjusted to compensate for the variable gain of the photodetectors. Figure 8 shows the swept output power from 8 to 12 GHz for the outputs from the four photodetectors at the wavelength of 1537 nm. The initial phase uniformity was achieved by using the electrical phase trimmers. The measured curves of phase difference versus modulation frequency at different wavelengths are shown in Fig. 9. The time delay between delay devices can be derived from the slope of each curve. The wavelength 1537 nm was chosen as a reference for zero time delay. By tuning the wavelength from 1537 to 1547 nm, different time delays can be achieved from 0 to 17 ps. To eliminate the nonlinear phase variation perturbation from the electrical part, the measurements described were made using the same photodetector. The linear curve of phase difference versus frequency verifies the true-time-delay and wide-bandwidth capability of the proposed scheme.

A four-element X-band phased array antenna system was also assembled. Figure 10 shows the characteristic S_{11} of one of the radiating elements, which emit most efficiently around the two frequencies 9 and 10 GHz. The radiation patterns of the four elements were measured at two different frequencies to verify the wide bandwidth of the wavelength-controlled phased array antenna system. The measured results are shown in Fig. 11(a) and 11(b). Figure 11(a) corresponds to the measurement at $\lambda = 1537$ nm with zero time delay between the delay modules. Figure 11(b) corresponds to the measurement at $\lambda = 1547$ nm with a scanning angle of 23 deg. For each wavelength, the patterns were measured at both frequencies. As expected, the measurement shows negligible beam squint effect in the assembled system.

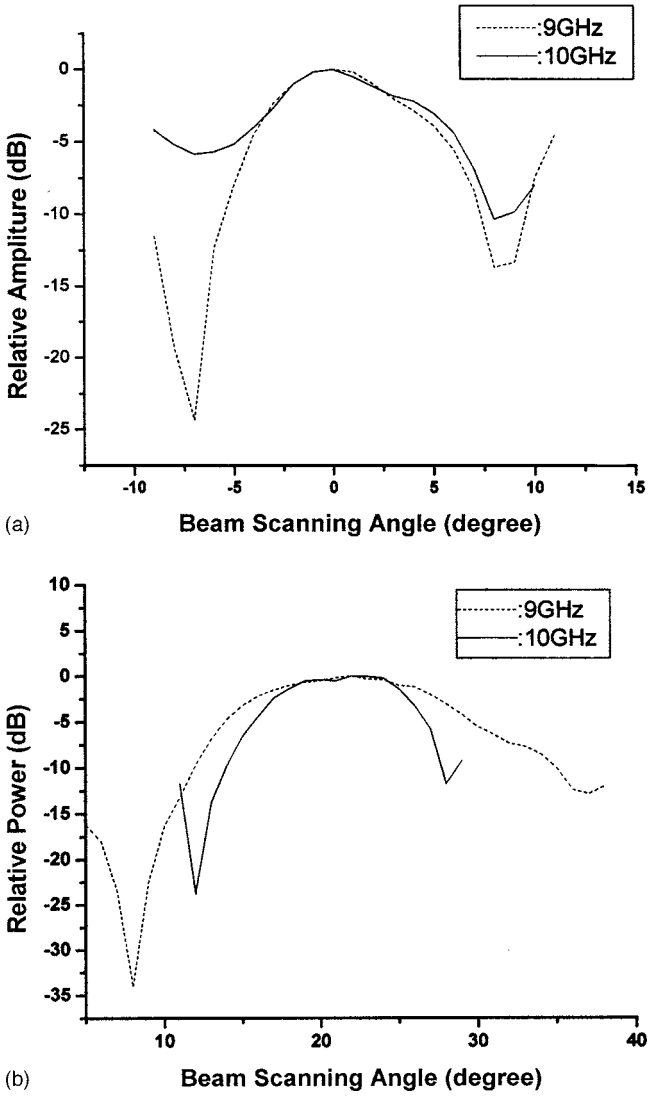

Fig. 11 Measured radiation patterns at 9 and 10 GHz, for (a) $\lambda = 1537$ nm, (b) $\lambda = 1547$ nm.

4 Conclusion

A four-element X-band phased array antenna system using hologram-waveguide-based true-time-delay modules has been proposed and experimentally implemented. The true-time-delay formation scheme and the experiment setup were described. The wavelength-controlled true time delays were measured across a 10-nm wavelength tuning range.

The radiation patterns of the antenna system at different frequencies were measured to verify the wide bandwidth of the experimental setup.

References

1. W. Ng, A. A. Walston, G. L. Tangonan, J. J. Lee, I. L. Newberg, and N. Bernstain, "The first demonstration of an optically steered microwave phased array antenna using true-time-delay," *J. Lightwave Technol.* **9**, 1124–1131 (1991).
2. E. H. Monsay, K. C. Baldwin, and M. J. Caucuitto, "Photonic true time delay for high-frequency phased array systems," *IEEE Photonics Technol. Lett.* **6**, 118–124 (1994).
3. M. Y. Frankel, R. D. Esman, and M. G. Parent, "Array transmitter/receiver controlled by a true time-delay fiber-optic beamformer," *IEEE Photonics Technol. Lett.* **7**(10), 1216–1218 (1995).
4. Z. Shi, Y. Jiang, B. Howley, F. Zhao, Y. Chen, and R. Chen, "Delay-time-tunable waveguide hologram modules for X-band phased array antenna," *IEEE Photonics Technol. Lett.* **15**, 972–974 (2003).
5. H. Kogelnik, "Coupled wave theory for thick hologram gratings," *Bell Syst. Tech. J.* **48**, 2909–2947 (1969).
6. R. Chen, S. Tang, M. M. Li, D. Gerald, and S. Natarajan, "1-to-12 surface normal three-dimensional optical interconnects," *Appl. Phys. Lett.* **63**, 1883–1885 (1993).

Biographies and photographs of authors not available.